Diffusive anisotropy in low-permeability Ordovician sedimentary rocks from the Michigan basin in southwest Ontario

Yan Xiang, Lisa Cavé, Diana Loomer & Tom Al*
Geology Department – University of New Brunswick, P.O. Box 4400, Fredericton, New Brunswick, Canada, E3B 5A3

ABSTRACT
Diffusive anisotropy was investigated by comparing the effective coefficient D_e of tracers on paired sub-samples, oriented normal (NB) and parallel to bedding (PB) prepared from freshly drilled rock cores. The X-ray radiography method using I^- tracer is effective for determination of D_e for samples with porosity > 2%, and through-diffusion (TD) measurements are used for the low-porosity limestone using I^- and HTO. The D_e values are on the order of 10^{-12} $m^{-2}{\cdot}s^{-1}$ for shale, 10^{-14} to 10^{-13} for siltstone, and 10^{-13} to 10^{-12} for limestone. The D_e values obtained using I^- tracer with samples in the PB orientation are approximately 1 to 4 times those obtained with the NB orientation and the anisotropy ratio (PB:NB) observed with HTO is in a range of 1 to 7. A method has been developed using $AgNO_3$ for fixation of I^- in the pores which allows for SEM visualization of pore connections and diffusion pathways in the samples.

RÉSUMÉ
L'anisotropie de la diffusion a été étudié en comparent les D_e obtenus pour des traceurs sur des pairs de sous-échantillons orientés normal (NB) et parallèle (PB) à la direction de déposition préparé à partir de carottes de roches. La radiographie au rayon X est efficace pour la détermination de D_e du traceur iodure (I^-) pour les échantillons ayant une porosité supérieure a 2%. Des mesures par « though-diffusion (TD)» ont été utilise pour les échantillons de « limestone » de base porosités en utilisant l'iodure ou l'eau enrichit au tritium (HTO) comme traceurs. Des valeurs de D_e de l'ordre de 10^{-12} $m^{-2}{\cdot}s^{-1}$ pour les échantillons de "shale", 10^{-14} to 10^{-13} pour les échantillons de « sillstone » et de 10^{-13} to 10^{-12} pour les échantillons de « limestone » ont été obtenu. Les valeurs de D_e obtenues en utilisant l'iodure pour les échantillons orientés PB sont approximativement 1 to 4 fois plus grande que les valeurs obtenues pour les échantillons orientés NB. L'anisotropie du rapport PB:NB observé avec le HTO varie entre 1 to 7. Une méthode utilisant $AgNO_3$ a été développé pour fixer l'iodure dans les pores après les mesures de diffusion qui permet l'utilisation de la microscopie électronique de balayage (SEM) pour visualiser la connexion des pores dans les échantillons.

Keywords: Effective diffusion coefficient D_e; Anisotropy; Iodide I^-; tritiated water (HTO); Shale; Limestone; Siltstone; Porosity; X-ray radiography; through-diffusion, SEM.

1 Introduction

Low-permeability sedimentary rocks have potential for use as natural barriers to solute transport from waste disposal facilities. In these rocks, mass transport is driven dominantly by diffusion under the influence of solute concentration gradients in pore water. In order to evaluate the suitability of these rock materials as barriers, laboratory investigations of the diffusion properties are required. Examples include the Opalinus clay in Switzerland (van Loon et al. 2003a,b), Callovo-Oxfordian argillite and mudrock in France (Bazer-Bachi et al. 2006; Melkior et al. 2004), shale and limestone in Canada (Cavé et al. 2009), and crystalline rock with porosity <1% in Canada (Vilks et al. 2003) and Sweden (Johansson et al. 1998). In-situ investigations at the field-scale have also been made on Opalinus clay in Switzerland (Soler et al. 2005; Wersin et al. 2004).

Solute transport by diffusion is a 3-dimensional phenomenon, and diffusive anisotropy must be taken into account. Van Loon et al. (2004) conducted through-diffusion measurements on the Opalinus clay in directions normal and parallel to bedding to determine the effective diffusion coefficients (D_e) of tritiated water (HTO), Na^+, Cl^- and I^- ions. Diffusion parallel to bedding (PB) was reported to be faster than diffusion normal to bedding (NB) by a factor of 4 to 6. Suzuki et al. (2004) studied anisotropy in D_e using HDO tracer in compacted bentonite and found that D_e values were greater by a factor of approximately 2 in the direction parallel to the preferred orientation of clay particles. Furthermore, the anisotropy ratio was found to be dependent on the dry density of compacted clay, with uncompacted bentonite reported to be isotropic (Sato and Suzuki 2003).

Studies of diffusive anisotropy have not been limited to layered sedimentary rocks. For example, working with rhyolite volcanic rocks, Yokoyama and Nakashima (2005) reported that the D_e of K^+ was 5 to 9 times greater in the direction parallel to layering than in the direction normal to layering. The anisotropic pore structure and pore connections in this rhyolite were demonstrated by SEM imaging. Similarly, Nishiyama et al. (1990) studied a

metamorphic schist and found that D_e values for I^- were 2 to 3 orders of magnitude larger in the direction parallel to the foliation, compared to the direction normal to the foliation.

The objective of this work was to measure the diffusion properties, including anisotropy, of limestone, shale and siltstone samples from a site under investigation for a deep geological repository (DGR) for low- and intermediate-level radioactive waste in Ontario, Canada.

2 Experimental Methods

The approach was to quantitatively determine D_e (HTO and I^- tracers), water-loss porosity and tracer-accessible porosity for paired sub-samples prepared in the NB and PB orientations. Diffusion measurements for shale samples with water-loss porosity between 8 to 12% were conducted using a relatively new technique, X-ray radiography (Tidwell et al. 2000; Cavé et al. 2009). For limestone samples with porosity between 0.7 to 2%, measurements were conducted using the through-diffusion (TD) method (van Loon et al. 2003a,b).

2.1 Sample Descriptions

The samples used in this study were obtained from three drill cores collected from a site in the Michigan Basin near Tiverton, Ontario. Samples representing the Ordovician period were selected from depths between 450 and 750 metres below surface in the sedimentary sequence (Table 1). The rocks in this range are mostly horizontally-bedded shales in the Upper Ordovocian and argillaceous limestones in the Middle Ordovician, both of which are characterized by low permeability. The samples represent a variety of lithologies occurring in the sequence, with some displaying local heterogeneity at the centimetre scale of the sub-samples used for diffusion measurements.

Samples from the upper Queenston Formation appear to be homogeneous, red-brown shales while those from around 520 m also contain minor green shale and thin layers of carbonate. Georgian Bay Formation shale samples are dark, mottled greenish-grey with minor fossil fragments. The upper part of the Georgian Bay Formation contains layers of siltstone and limestone that are several centimetre thick, decreasing in thickness and frequency with depth. Some of these interbeds are present in the diffusion test samples. The Blue Mountain Formation is represented in this data set by a single sample of dark blue-grey shale.

The limestone samples are more heterogeneous than the shales. Samples from the Cobourg and Sherman Fall Formations are typically light grey, mottled, hard limestones and argillaceous limestones, with abundant small invertebrate fossils and very low porosity. Thin grey shale interbeds and shaley partings (less than 1 cm) are present in some of the samples. The Sherman Fall Formation also contains slightly thicker dark grey calcareous shale interlayers (Armstrong and Carter 2006), but these are not represented in this sample set.

Table 1. Stratigraphy, lithology and depth for samples collected from three boreholes DGR2, DGR3 and DGR4.

System	Formation	Lithology	Depth of drill core samples (m)		
			DGR2	DGR3	DGR4
Upper Ordovician	Queenston	Red shale	457	468	
			518	525	
	Georgian Bay	Siltstone	544		
			562		
		Grey shale	594	563	
			596	608	
	Blue Mountain	Grey shale		641	
Middle Ordovician	Cobourg (Lower Member)	Calcareous shale and argillaceous limestone	677	672	661
				675	671
				681	
				688	
				691	
	Sherman Fall	Limestone		725	719

2.2 Pore Water Composition

Synthetic pore water (SPW) solutions were formulated for use in the diffusion experiments (Sections 2.4 and 2.5 below) in order to match the composition and ionic strength of the natural pore water, and thereby eliminate the influence of osmotic gradients. SPW solutions were also used in porosity measurements (Section 2.3). The chemical compositions of natural pore water in rock core samples were estimated using a crush-and-leach method on a total of 6 samples, representing three different rock types: red shale, grey shale and limestone.

Samples saturated with natural pore water were first crushed coarsely, and oven dried at 40°C for 6 days. Crushed samples were milled and sieved to particle size <105 μm, then dried again at 40°C to a constant mass. Samples were weighed into plastic bottles, a known mass

of de-ionized water was added, and they were agitated on a rotating or wrist-action shaker for 48 hours. After allowing solids to settle over night, the supernatant liquid was filtered (0.45 μm) prior to chemical analysis for major cations (ICP-AES) and anions (IC) at the New Brunswick Research and Productivity Council. The concentration of ions present in rock pore water is estimated using the following equation:

$$C_{pw} = \frac{C_{rock} \cdot \rho_{gr} \cdot (1-\phi_W)}{\phi_W} \quad (1)$$

where C_{pw} is the concentration estimate for the ion of interest (mol·L^{-1}) in the pore water; C_{rock} is the ion concentration present in mol·kg^{-1} rock (based on aqueous leaching and chemical analysis); ρ_{gr} is the average grain density of the rock material; ϕ_w is the water-loss porosity of the rock. The values of ρ_{gr} and ϕ_w were determined gravimetrically as described in Section 2.3 below.

Equation 1 assumes that ions leached from crushed rock were originally present in the natural pore water. However, soluble evaporite minerals such as halite and anhydrite are known to occur in these rocks, and the equilibrium geochemical model, PHREEQC, was used with the Pitzer.dat database to investigate the saturation state of the estimated pore water composition with respect to evaporite minerals. In cases where simulations suggested the solutions are over saturated with respect to one or more evaporite minerals, the model was used to calculate the reduction in concentration required to bring the solutions to saturation. Reduction of Ca^{2+} and SO_4^{2-} concentrations were required in all cases to bring the solutions to equilibrium with respect to anhydrite.

2.3 Water-loss Porosity, ϕ_w

Measurements of ϕ_w are used for comparison with tracer-accessible porosity determinations from the diffusion experiments. Experimental procedures for the water-loss method used in this work are consistent with that of Blum (1997) such that the measurements account for the high salinity of the pore water.

Samples were received saturated with natural pore water. Immediately after sub-sampling, the mass of the saturated sample was determined while the sample was submerged in SPW. The beaker containing SPW was then removed and the mass of the sample was determined repeatedly over time to plot a surface drying curve. The mass of the saturated, surface-dry sample was determined at the inflection point of slope change, indicating a change from surface evaporation to pore fluid evaporation. Samples were then oven-dried at 105°C and the mass monitored over several weeks. The final dry mass was then recorded when a constant mass was obtained. The water-loss porosity and grain density were calculated using the following equations:

$$V_{rock} = \frac{M_{sat} - M_{sub}}{\rho_{SPW}} \quad (2)$$

$$V_{voids} = \frac{M_{sat} - M_{dry}}{(1-x)\,\rho_{SPW}} \quad (3)$$

$$\phi_w = \frac{V_{voids}}{V_{rock}} \times 100\% = \frac{M_{sat} - M_{dry}}{(1-x)[M_{sat} - M_{sub}]} \times 100\% \quad (4)$$

$$\rho_{gr} = \frac{M_{rock}}{V_{rock} - V_{voids}} \quad (5)$$

$$M_{rock} = M_{dry} - M_{salt} = M_{dry} - V_{voids} \cdot \rho_{SPW} \cdot x \quad (6)$$

where M_{sat} is the mass of the saturated, surface-dry sample weighed in air; M_{sub} is the mass of the saturated sample weighed by suspension when submerged in SPW; M_{dry} is the mass of the oven-dried sample (including salts retained in voids) weighed in air; ρ_{gr} is the average grain density of the rock sample; ρ_{SPW} is the density of the SPW which was determined experimentally; and x is the mass fraction of the salts in SPW. Because of the high salinity of the SPW, an accurate mass of a dry rock sample can only be obtained when the mass of the salts retained in voids after drying (M_{salt}) are subtracted from M_{dry}. This method assumes that the density and mass fraction of salts of the SPW and the natural pore water are equal.

2.4 X-ray Radiography Diffusion Experiments

The principle, methodology, experimental procedures, and data processing for diffusion measurements by X-ray radiography used in this research are described by Cavé et al. (2009). Briefly, the cylindrical sub-cores (11 mm diameter, 15 to 20 mm length) were brushed with a thin coat of silicone, enclosed in heat-shrink tubing (3M FP-301) and then attached to the reservoirs of the diffusion cells (Figure 1). The samples were saturated for at least 3 weeks in SPW, after which a disc of aluminum or ceramic was placed on top of each saturated rock cylinder. The disc is used as an internal standard to correct for inconsistencies in the X-ray source.

Diffusion experiments were initiated by filling the reservoirs of the diffusion cells with 1.0 M NaI tracer solution (Table 3) and covering the injection holes. Reference radiographs were collected immediately after tracer solution was injected. Samples were stored at 22 ± 1 °C in a closed container with an open dish of water to maintain equilibrium vapour pressure and prevent evaporative drying of the samples. Time-series radiographs were typically collected at intervals of 1 to 4 days, starting 18 hrs after the tracer was added, and continuing until iodide breakthrough occurred at the top end of the samples (up to 504 hrs). During this time the tracer solutions in the reservoirs were refreshed periodically. After iodide breakthrough, the samples were saturated with NaI tracer from both ends by removing the nylon screws in the discs and submerging in 1.0 M NaI

tracer solution. The progress of saturation is monitored by X-ray radiography until no changes are observed in X-ray attenuation between consecutive images. A time period of 3 to 4 weeks was required to saturate the samples, after which time the final radiographs for the tracer-saturated samples were collected.

All data were collected as digital radiographs using a Skyscan 1072 desktop microCT instrument.

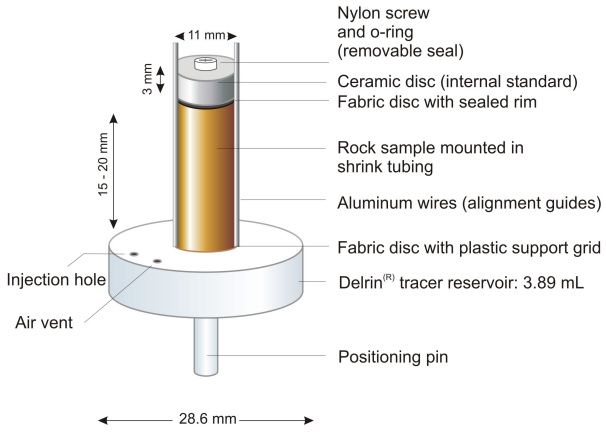

Figure 1. Diagram of the diffusion cell used for diffusion experiments by X-ray radiography

2.5 Through-diffusion

Through-diffusion measurements were based on the method of van Loon (2003a,b). Modifications of cell design and experimental set-up have been made to suit this work. Samples were either 25.4 or 76.0 mm diameter and 10 mm thick. Diffusion measurements on all samples with PB orientation were made using a 25.4 mm-diameter cell design and the measurements on samples with NB orientation were made using either the 25.4 or 76.0 mm-diameter cell design (Figure 2).

The circumference of the samples was brushed with a thin layer of silicone, delrin plugs, with several small plastic spacers attached to create a reservoir for circulation of the fluid, were set in place at each end and a heat-shrink clamp (PowerGrip, McMaster-Carr) was placed around the perimeter of the sample and the delrin plugs (see Figure 2). The cell was assembled by activating the shrink clamp, and then a steel gear clamp was tightened around the circumference of the heat-shrink clamp to ensure a seal around the perimeter of the sample.

The dead volume in each side of the diffusion cells was measured by injecting SPW with a syringe. The cell was then tested by applying a fluid pressure to the ports on one side using a syringe filled with SPW. After passing the leakage test, the cell was attached to containers of tracer solution (high concentration side) and SPW (low concentration side), and a peristaltic pump (205U Watson Marlow or Ecoline VC-MS/CAB-6, Ismatec), via fluoropolymer tubing. The speed of the pump was adjusted to 25 mL·hr^{-1}.

Although samples were prepared from cores that were received saturated with natural pore water, some drying may occur at the outer surfaces during assembly of the diffusion cells. Samples were re-saturated by circulating SPW solution in both reservoirs for at least 3 weeks prior to starting the experiments. Following the saturation period, SPW in the lower reservoir was replaced by tracer solution so that the direction of tracer flux or diffusion was from bottom to top.

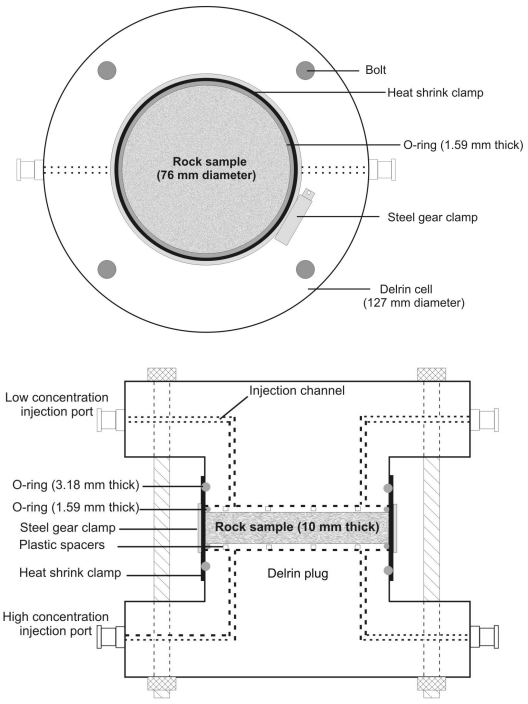

Figure 2. Diagrams of 76-mm TD cell: cross-section (top) and side view (bottom).

The tracer mass flux across the large surface area of the 76-mm samples is greater than that across the 25.4-mm samples. Similarly, the shale samples have higher porosity and therefore permit a greater tracer flux across the samples than is the case for limestone and siltstone. The tracer concentration gradients were adjusted accordingly (Table 2) in order to satisfy the requirement for low concentrations at the out-flux boundary. The volume of the tracer solution was chosen such that the estimated mass of tracer that diffused through the rock sample over the time period of the experiment (up to 80 days) was less than 1% of the tracer mass initially present in the high concentration reservoir.

Each low concentration reservoir contained a known volume of SPW solution, typically 15-40 mL, adjusted depending on the flux through the samples. The quantity of I^- (mmol) that diffused through the samples was determined by an Ion Selective Electrode (combined ISE, London Scientific Limited). The electrode was calibrated

using a series of standard solutions at each use. The quantity of HTO (in Bq) that diffused through the samples was determined by liquid scintillation counting (LS 6000 Series, Beckman; BCS scintillation cocktail, GE Healthcare). Diffusion data were typically collected in time intervals of 2 to 4 days. Fresh SPW solutions of known volumes were replaced in the low concentration reservoirs after each sampling. The quantity of the tracer that remained in the tubing and in the dead volume of the cell was accounted for in data calculations. All the joints of the cells were airtight and the cells were maintained in the open atmosphere in the laboratories at 22±1.5ºC for NaI and 21.5±1.5ºC for HTO diffusion experiments.

Table 2. Tracer solutions used in TD experiments.

Cell Size/ Rock Type	NaI Tracer [a]		HTO Tracer [a]	
	Conc. (M)	Volume (mL)	Conc. (Bq/mL)	Volume (mL)
25.4 mm shale	1.0	200	5000	200
25.4 mm limestone	1.0	40	50,000	40
76.0 mm limestone	0.2	200	10,000	200

[a] All tracer solutions were prepared in SPW matrix (see Table 3).

For each TD experiment, the flux of the tracer (mmol·m^{-2}·day^{-1} for iodide or Bq·m^{-2}·day^{-1} for HTO) and the total accumulated mass of the tracer that diffused through the sample are plotted as a function of time (Figure 3). The approach to steady-state is represented by an asymptotic increase on the plot of flux versus time (Figure 3) and by a linear increase in cummulative tracer mass vs. time (Figure 3). The values of D_e and rock capacity factor (α) are derived from the slope and intercept, respectively, of the linear portion of the tracer mass vs time curve. When a conservative tracer is used in the experiment, the α value obtained by this method represents the tracer-accessible porosity (van Loon et al. 2003a,b).

2.6 SEM Imaging

After the completion of diffusion experiments in which I^- was used as a tracer, rock samples were immersed in $AgNO_3$ solution (0.1 M) for six days to allow Ag^+ ions to diffuse into the pores and fix the I^- ions in place by the precipitation of AgI. The samples were then sectioned parallel to the diffusion path and polished thin sections were prepared for SEM analysis. Back scattered electron images (BSEI) and elemental maps were collected to visualize the distribution of AgI, and thereby provide evidence of the diffusion pathways in the sample. The SEM images were recorded at the Microscopy and Microanalysis Facility at UNB using a JEOL JSM6400 Scanning Electron Microscope equipped with an EDAX Genesis Energy Dispersive X-ray Spectroscopy (EDS) system.

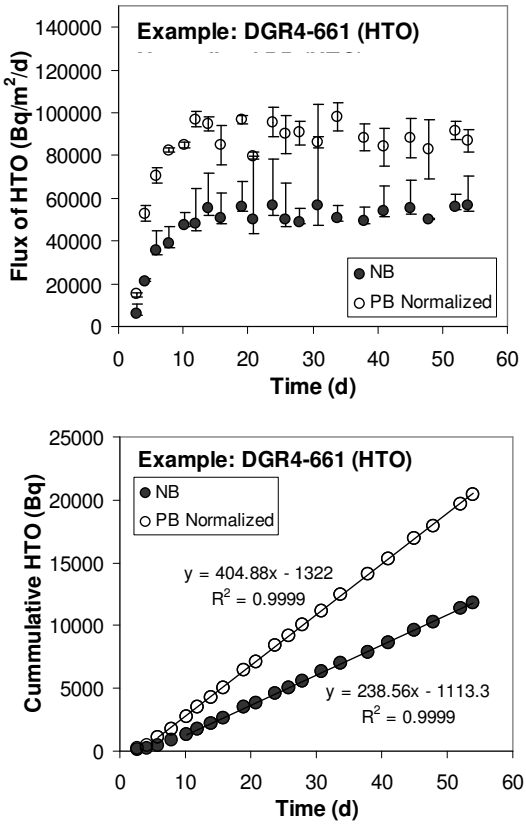

Figure 3. Examples of HTO flux versus time (top) and cumulative HTO mass versus time (bottom) obtained from TD experiments. The data for samples with PB orientation are normalized to the same tracer concentration gradient as was used for samples with NB orientation.

3 Results and Discussion

Two SPW compositions were formulated based on the estimated pore water compositions determined for shale and limestone (Table 3). The salinity of the synthetic pore water is high, up to 5.8 M and 3.8 M Cl^- for shale (S-SPW hereafter) and limestone (L-SPW hereafter), respectively. Table 3 also presents the compositions of NaI tracer solutions prepared for use in the diffusion experiments.

Although tracer accessible porosity values determined by TD are reported (Table 5), it is known that TD is not a sensitive method for determination of tracer-accessible porosity (van Loon et al. 2003a). We therefore restrict our discussion of porosity to ϕ_w values determined gravimetrically, and ϕ_I values determined by radiography (Table 4).

Measurements of ϕ_w range from 8 to 12% for shale, from 2 to 3.5% for siltstone, and from 0.7 to 2% for limestone (Tables 4 and 5). These measurements represent a bulk value and, although they provide some indication of the heterogeneous distribution of porosity at the formation scale, they provide no information on the heterogeneity

that exists at the sample scale. Similarly α values determined by the TD method is also a bulk value and provides no information on heterogeneity at the scale of the sample. In contrast, the diffusion accessible porosity determined by the radiography method, ϕ_I, is spatially resolved, and reflects the spatial variability in porosity at the sample scale (Figure 4). These data indicate that porosity in many of the DGR rock samples is heterogeneously distributed, and this is particularly evident from measurements made across bedding in the NB orientation. Given that porosity and D_e are thought to be related through Archie's law (Boving and Grathwohl 2001), the bedding related variability in porosity is expected to give rise to anisotropy in diffusion properties.

Table 3. Compositions of SPW and NaI tracer solutions used with diffusion experiments.

	Shale SPW (mol/L)	Shale NaI Tracer (mol/L)	Limestone SPW (mol/L)	Limestone NaI Tracer (mol/L)
NaCl	2.4	1.4	2.0	1.0
KCl	0.50	0.50	0.45	0.45
$CaCl_2.2H_2O$	1.2	1.2	0.48	0.48
$MgCl_2.6H_2O$	0.25	0.25	0.20	0.20
$CaSO_4$	0.0010	0.0010	0.0050	0.0050
NaI	0	1.0	0	1.0

Table 4. Summary of D_e and ϕ_I determined by radiography and ϕ_w data.

Formation/ Rock Type	Sample ID [a]	Water-loss porosity, ϕ_w	NaI tracer [b]		
			D_e (m^2/s)	ϕ_I	D_e ratio (PB/NB)
Queenston Red Shale	DGR2-457-NB	0.090	1.8×10^{-12}	0.04	2.2
	DGR2-457-PB		4.0×10^{-12}	0.047	
	DGR2-518-NB	0.078	1.5×10^{-12}	0.037	1.7
	DGR2-518-PB		2.5×10^{-12}	0.035	
	DGR3-468-NB	0.109	2.4×10^{-12}	0.042	1.2
	DGR3-468-PB		2.8×10^{-12}	0.051	
	DGR3-525-NB	0.084	9.7×10^{-13}	0.033	2.6
	DGR3-525-PB		2.5×10^{-12}	0.041	
Georgian Bay Siltstone	DGR2-544-NB	0.035	8.5×10^{-14}	0.014	2
	DGR2-544-PB		1.7×10^{-13}	0.014	
	DGR2-562-NB	0.020	4.1×10^{-14}	--	1.9
	DGR2-562-PB		7.8×10^{-14}	0.008	
Georgian Bay Grey Shale	DGR3-563-NB	0.121	1.4×10^{-12}	0.054	3.8
	DGR3-563-PB		5.3×10^{-12}	0.059	
	DGR2-594-NB	0.092	1.1×10^{-12}	0.041	3.3
	DGR2-594-PB		3.6×10^{-12}	0.048	
	DGR2-596-NB	0.083	1.4×10^{-12}	0.039	3.6
	DGR2-596-PB		5.0×10^{-12}	0.067	
	DGR3-608-NB	0.092	4.8×10^{-13}	0.041	4.8
	DGR3-608-PB		2.3×10^{-12}	0.043	
Blue Mountain Grey Shale	DGR3-641-NB	0.090	7.6×10^{-13}	0.042	4.1
	DGR3-641-PB		3.1×10^{-12}	0.039	
Cobourg Limestone	DGR2-677-NB	0.021	4.2×10^{-13}	0.01	2.1
	DGR2-677-PB		9×10^{-13}	0.015	

NOTES: [a] DGRX-YYY-ZZ: drill hole X, depth Y (m) and orientation Z (PB or NB); [b] C_0 = 1.0 M NaI prepared in S-SPW matrix, except for DGR2-677 prepared in L-SPW matrix.

Table 5. Summary of D_e and α determined by TD using NaI and HTO tracers and ϕ_w data

Formation/ Rock type	Sample ID [a]	ϕ_w	NaI tracer [b]			HTO tracer [b]			D_e ratio (HTO/NaI)
			D_e (m^2/s)	α_I	D_e ratio (PB/NB)	D_e (m^2/s)	α_{HTO}	D_e ratio (PB/NB)	
Georgian Bay Siltstone	DGR2-544-NB	0.035	1.2×10^{-13}	0.02	2.7	--	--	--	--
	DGR2-544-PB		3.2×10^{-13}	0.025		--	--		--
Cobourg Limestone	DGR4-661-NB	0.0099	--	--	--	6.8×10^{-13}	0.012	1.8	--
	DGR4-661-PB		--	--		1.2×10^{-12}	0.014		--
	DGR4-671-NB	0.0123	3.8×10^{-13}	0.013	1.2	--	--	--	--
	DGR4-671-PB		4.7×10^{-13}	0.01		--	--		--
	DGR3-672-NB	0.0106	*4.8×10^{-13}*	*0.017*	1.1	7.9×10^{-13}	0.014	1.1	1.65
	DGR3-672-PB		5.3×10^{-13}	*0.015*		*8.5×10^{-13}*	*0.012*		1.60
	DGR3-675-NB	0.0091	*2.5×10^{-13}*	*0.01*	1.7	3.2×10^{-13}	0.006	3.1	1.28
	DGR3-675-PB		4.3×10^{-13}	*0.012*		*1.0×10^{-12}*	*0.012*		2.33
	DGR3-681-NB	0.0129	*4.5×10^{-13}*	*0.017*	1.6	7.8×10^{-13}	0.012	2.4	1.73
	DGR3-681-PB		7.1×10^{-13}	*0.017*		*1.9×10^{-12}*	*0.021*		2.68
	DGR3-688-NB	0.019	*2.1×10^{-13}*	*0.005*	4.2	3.3×10^{-13}	0.005	7	1.57
	DGR3-688-PB		8.8×10^{-13}	*0.02*		*2.3×10^{-12}*	*0.021*		2.61
	DGR3-691-NB	0.0069	*4.2×10^{-13}*	*0.009*	0.9	3.3×10^{-13}	0.004	1.5	0.79
	DGR3-691-PB		3.9×10^{-13}	*0.004*		*4.9×10^{-13}*	*0.004*		1.26
Sherman Fall Limestone	DGR4-719-NB	0.0177	--	--	--	1.6×10^{-12}	0.02	1.1	--
	DGR4-719-PB		--	--		1.8×10^{-12}	0.018		--
	DGR3-725-NB	0.0072	*3.0×10^{-13}*	*0.004*	1.9	8.0×10^{-13}	0.011	1.3	2.67
	DGR3-725-PB		5.8×10^{-13}	*0.008*		*1.0×10^{-12}*	*0.007*		1.72

NOTES: [a] DGRX-YYY-ZZ: drill hole X, depth Y (m) and orientation Z (NB or PB); [b] prepared in L-SPW matrix except for DGR2-544 prepared in S-SPW matrix (see Table 2 for concentrations).

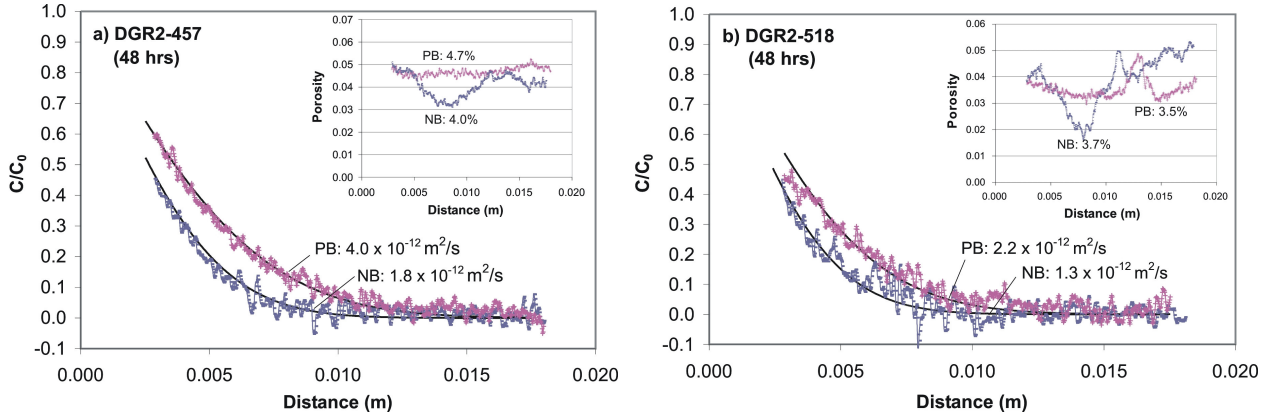

Figure 4. 1-D profiles of ϕ_I and relative iodide concentration (C/C_0) obtained with X-ray radiography for paired shale samples prepared in the NB and PB orientations.

The profiles of ϕ_I (Figure 4) have been integrated with respect to distance to obtain an average value for each sample (Table 4). Comparison of the average ϕ_I values with ϕ_w data indicates that ϕ_I values are systematically lower (40% to 60%). This difference is likely related to anion exclusion (Melkior et al. 2004; Bazer-Bachi et al. 2006; van Loon et al. 2003 a,b; 2007) as most of the ϕ_I measurements are made in the clay-rich shales, and even the limestone samples contain argillaceous sections.

The D_e values for NaI tracer range from 4.8 x 10^{-13} to 5.3 x 10^{-12} $m^{-2}{\cdot}s^{-1}$ for shale, 4.1 x 10^{-14} to 3.2 x 10^{-13} $m^{-2}{\cdot}s^{-1}$ for siltstone, and 2.1 x 10^{-13} to 9.0 x 10^{-13} $m^{-2}{\cdot}s^{-1}$ for limestone, which are in good agreement with the data reported by Cavé et al. (2009). The data provide indications of bedding related anisotropy, and in general, the D_e values for I^- and HTO tracers in the PB orientation are larger than the D_e values for the NB orientation (Tables 4 and 5; Figures 3 to 5). The anisotropy ratio for D_e values in the PB versus the NB orientation varies from 1.2 to 4.8 for shale samples, 1.9 to 2.7 for siltstone, and 0.9 to 7 for limestone. The origin of this anisotropy is believed to relate to directional differences in pore connectivity in these porous media. The SEM imaging provides some evidence for this difference in connectivity (Figure 6). The bright regions in the BSEI represent AgI precipitates (Figure 7) formed by the addition of $AgNO_3$ to the I^--containing samples following the diffusion experiments. The images therefore illustrate anisotropy in diffusive pathways for I^- tracer in the pores.

The data also indicate tracer-related differences in D_e, and although TD measurements were not conducted on shale and siltstone samples, the D_e values for limestone using HTO tracer are larger than those for the I^- tracer, ranging from 3.2 x 10^{-13} to 2.3 x 10^{-12} $m^{-2}s^{-1}$ (Table 5; Fig. 5). The lower D_e and ϕ_I values for I^- tracer are consistent in supporting the inference that I^- transport in these rocks is affected by anion exclusion.

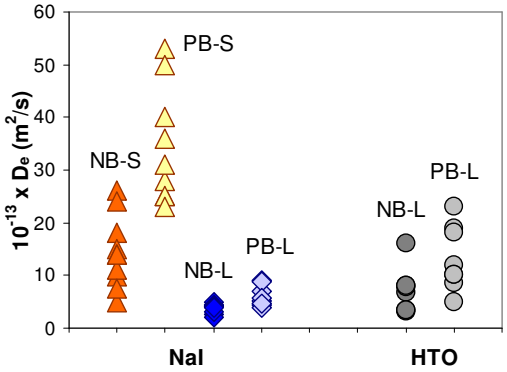

Figure 5. Compilation of D_e data from radiography and TD experiments illustrating the differences among rock types, tracers and measurement orientations (Δ = shale with iodide tracer, ◊ = limestone/siltstone with iodide tracer, O = limestone/siltstone with HTO tracer).

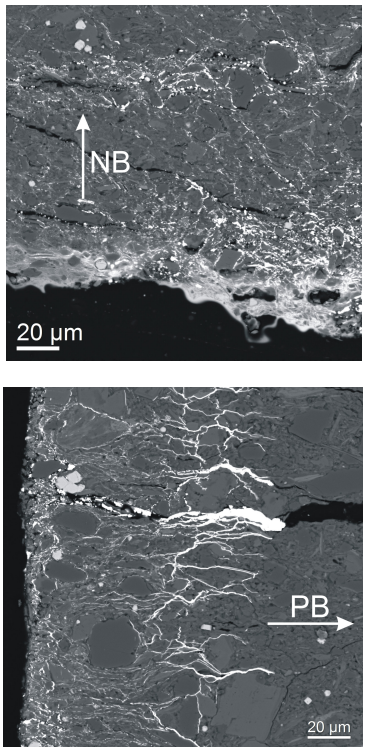

Figure 6. Back scattered electron images (BSEI) of DGR2-596 grey shale showing the distribution of AgI precipitate in the pores in the NB and PB directions.

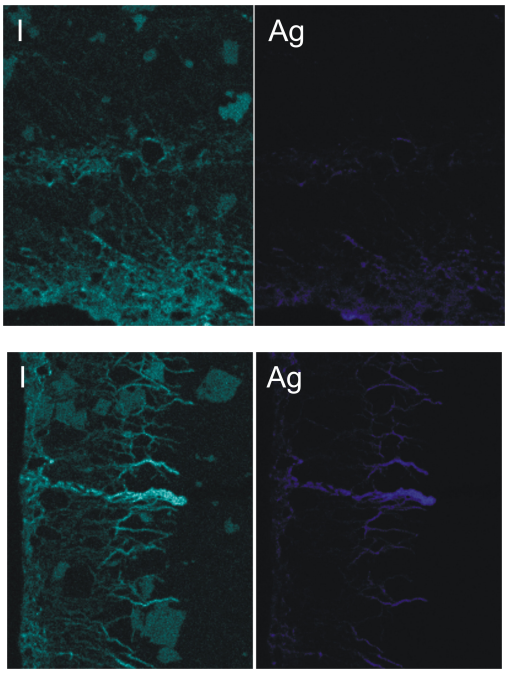

Figure 7. Element maps acquired by Energy-dispersive X-ray spectroscopy: NB (top) and PB (bottom) showing iodine and silver distributions in DGR2-596.

4 Acknowledgements

This work was supported by funding from the Nuclear Waste Management Organization (NWMO) and Ontario Power Generation. Radiography was assisted by J. Bowles, S. Thangavelu and P. Arsenault, Mechanical Engineering, UNB. Dr. Esam Hussein (UNB, Mech. Eng.) provided helpful comments and Dr. Monique Hobbs (NWMO) contributed to the design and review of the project. Dr. David Kubien and Dr. Dion Durnford, Biology, UNB, allowed access to their laboratory where HTO experiments were conducted. SEM work was assisted by Dr. Douglas Hall, Microscopy and Microanalysis Facility, University of New Brunswick.

5 References

Altman, S.J., Uchida, M., Tidwell, V.C., Boney, C.M. and Chambers, B.P. 2004. Use of X-ray absorption imaging to examine heterogeneous diffusion in fractured crystalline rocks, *Journal of Contaminant Hydrology*, 69: 1-26.

Armstrong, D.K. and Carter, T.R. 2006. *An updated guide to the subsurface Paleozoic stratigraphy of Southern Ontario*, Open File report 6191, Ontario Geological Survey, Ontario, Canada.

Bazer-Bachi, F., Tevissen, E., Descostes, M., Grenut, B., Meier, P., Simonnot, M.-O. and Sardin, M. 2006. Characterization of iodide retention on Callovo-Oxfordian argillites and its influence on iodide migration, *Physics and Chemistry of the Earth,* 31: 517-522.

Blum, P. 1997. *Physical properties handbook: a guide to the shipboard measurement of physical properties of deep-sea cores,* ODP Tech. Note 26, Ocean Drilling Program, Texas, USA.

Boving, T.B. and Grathwohl, P. 2001. Tracer diffusion coefficients in sedimentary rocks: Correlation to porosity and hydraulic conductivity, *Journal of Contaminant Hydrology*, 53: 85-100.

Cavé, L., Al, T., Xiang, Y. and Vilks, P. 2009. A technique for estimating one-dimensional diffusion coefficient in low-permeability sedimentary rock using X-ray radiography: Comparison with through-diffusion measurements, *Journal of Contaminant Hydrology*, 103: 1-12.

Johansson, H., Siitari-Kauppi, M., Skålberg, M. and Tullborg, E.L. 1998. Diffusion pathways in crystalline rock – examples from Äspö-diorite and fine-grained granite, *Journal of Contaminant Hydrology*, 35: 41-53.

Melkior, T., Mourzagh, D., Yahiaoui, S., Thoby, D., Alberto, J.C., Brouard, C. and Michau, N. 2004. Diffusion of an alkaline fluid through clayey barriers and its effect on the diffusion properties of some chemical species, *Applied Clay Science,* 26: 99-107.

Nishiyama, K., Nakashima, S., Tada, R. and Uchida, T. 1990. Diffusion of an ion in rock pore water and its relation to pore characteristics, *Mining Geology,* 40: 323-336 (in Japanese, with English abstract).

Sato, H. 2001. The effect of pore structural factors on diffusion in compacted sodium bentonite. In: Hart, K.P. and Lumpkin, G.R. (eds.), *Materials Research Society Symposium Proceedings*, 663: 605-615.

Sato, H. and Suzuki, S. 2003. Fundamental study on the effect of an orientation of clay particles on diffusion pathway in compacted bentonite, *Applied Clay Science,* 23: 51-60.

Shackelford, C.D. 1991. Laboratory diffusion testing for waste disposal – A review, *Journal of Contaminant Hydrology*, 7: 177-217.

Soler, J.M., Gimmi, T., Cartalde, A., Wersin, P. and van Loon, L.R. 2005. In-situ diffusion at Mont Terri URL, *Geochimica et Cosmochimica Acta,* 69 (10) Suppl.: 175.

Suzuki, S., Sato, H., Ishidera, T. and Fujii, N. 2004. Study on anisotropy of effective diffusion coefficient and activation energy of deuterated water in compacted sodium bentonite, *Journal of Contaminant Hydrology*, 68: 23-37.

Tidwell, V.C., Meigs, L.C., Christian-Frear, T. and Boney, C.M. 2000. Effects of spatially heterogeneous porosity on matrix diffusion as investigated by X-ray absorption imaging, *Journal of Contaminant Hydrology*, 42: 285-302.

van Loon, L.R., Glaus, M.A., and Muller W. 2007 Anion exclusion effects in compacted bentonites: Towards a better understanding of anion diffusion, *Applied Geochemistry*, 22: 2536-2552.

van Loon, L.R, Soler, J.M. and Bradbury, M.H. 2003a. Diffusion of HTO, $^{36}Cl^-$ and $^{125}I^-$ in Opalinus Clay samples from Mont Terri: Effect of confining pressure, *Journal of Contaminant Hydrology*, 61: 73-83.

van Loon, L.R., Soler, J.M., Jakob, A. and Bradbury, M.H. 2003b. Effect of confining pressure on the diffusion of HTO, $^{36}Cl^-$ and $^{125}I^-$ in a layered argillaceous rock (Opalinus Clay): Diffusion perpendicular to the fabric, *Applied Geochemistry*, 18: 1653-1662.

van Loon, L.R., Soler, J.M., Müller, W. and Bradbury, M.H. 2004. Anisotropic diffusion in layered argillaceous rocks: A case study with Opalinus Clay, *Environmental Science and Technology*, 38: 5721-5728.

Vilks, P., Cramer, J., Jensen, M., Miller, N., Miller, H. and Stanchell, F. 2003. In situ diffusion experiment in granite: Phase I, *Journal of Contaminant Hydrology*, 61: 191-202.

Wersin, P., van Loon, L.R., Soler, J.M., Yllera, A., Eikenberg, J., Gimmi, T., Hernán, P. and Boisson, J.-Y. 2004. Long-term diffusion experiment at Mont Terri: First results from field and laboratory data, *Applied Clay Science,* 26: 123-135.

Yllera, A., Hernández, A., Mingarro, M., Quejido, A., Sedano, L.A., Soler, J.M., Samper, J., Molinero, J., Barcala, J.M., Martin, P.L., Fernández, M., Wersin, P., Rivas, P. and Hernán, P. 2004. DI-B experiment: Planning, design and performance of an in situ diffusion experiment in the Opalinus Clay formation, *Applied Clay Science*, 26: 181-196.

Yokoyama, T. and Nakashima, S. 2005. Diffusivity anisotropy in a rhyolite and its relation to pore structure, *Engineering Geology*, 80: 328-335.